

Knowledge Distillation via Virtual Relation Matching

Weijia Zhang¹ Fei Xie¹ Weidong Cai² Chao Ma¹

¹Shanghai Jiao Tong University ²University of Sydney

{weijia.zhang, jaffe031, chaoma}@sjtu.edu.cn, {tom.cai}@sydney.edu.au

Abstract

Knowledge distillation (KD) aims to transfer the knowledge of a more capable yet cumbersome teacher model to a lightweight student model. In recent years, relation-based KD methods have fallen behind, as their instance-matching counterparts dominate in performance. In this paper, we revive relational KD by identifying and tackling several key issues in relation-based methods, including their susceptibility to overfitting and spurious responses. Specifically, we transfer novelly constructed affinity graphs that compactly encapsulate a wealth of beneficial inter-sample, inter-class, and inter-view correlations by exploiting virtual views and relations as a new kind of knowledge. As a result, the student has access to rich guidance signals and stronger regularisation throughout the distillation process. To further mitigate the adverse impact of spurious responses, we prune the affinity graphs by dynamically detaching redundant and unreliable edges. Extensive experiments on CIFAR-100 and ImageNet datasets demonstrate the superior performance of the proposed virtual relation matching (VRM) method over a range of models, architectures, and set-ups. For instance, VRM for the first time hits 74.0% accuracy for ResNet50→MobileNetV2 distillation on ImageNet, and improves DeiT-Ti by 14.44% on CIFAR-100 with a ResNet56 teacher. Thorough analyses are also conducted to gauge the soundness, properties, and complexity of our designs. Code and models will be released.

1. Introduction

Deep learning is achieving incredible performance at the cost of increasing model complexity and overheads. As a consequence, large and cumbersome neural models struggle to work in resource-constrained environments. Knowledge distillation (KD) has been proposed by [24] to address this issue by transferring the knowledge of larger and more capable models to smaller and lightweight ones that are resource-friendly. KD works by minimising the distance between compact representations of knowledge extracted from the teacher and student models. It has found

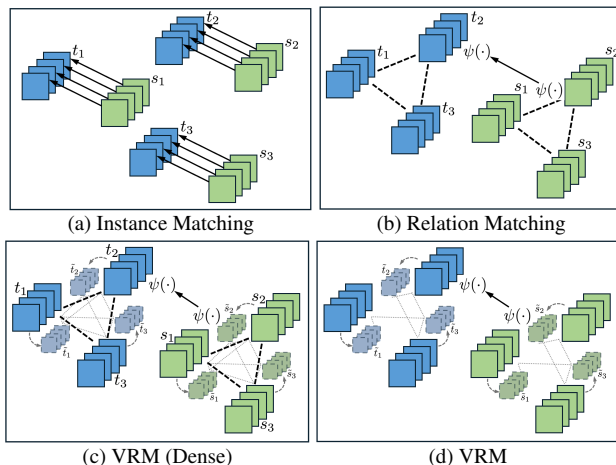


Figure 1. Conceptual illustration of VRM compared to existing KD methods based on instance matching and relation matching.

widespread application across a spectrum of downstream tasks [16, 20, 27, 30, 53, 56, 57, 60, 65, 67, 70].

According to the type of knowledge representations used for transfer, KD methods can be broadly categorised into feature-based [46], logit-based [24], and relation-based [43] approaches. The former two directly match the feature maps or logit vectors produced by the teacher and student models for each training sample, which is essentially *instance matching* (IM). By contrast, *relation matching* (RM) methods construct and match structured relations extracted within a batch of model responses. A conceptual illustration is presented in Figs. 1a and 1b.

Instance matching has been the prevailing distillation approach in recent years. Popular KD benchmarks see a dominance by IM methods such as FCFD [37], NORM [39], and TGeoKD [25], with different downstream tasks successfully tackled by directly adopting IM-based distillation [4, 12, 53, 59]. Yet, recent studies discovered that relational knowledge is more robust to variations in neural architectures, data modalities, and tasks [43, 52]. Meanwhile, methods transferring relations have also achieved promising performance for a range of tasks, including but not limited to segmentation [57] and detection [13, 28].

Despite growing interest, relation-based methods still

fall significantly short compared to their instance matching counterparts. Even the strongest RM method has been outperformed easily by recent IM solutions [26] (see Tabs. 1 and 2). RM-based methods also struggle with more challenging tasks such as object detection [26]. Moreover, previous RM solutions are primarily limited to matching inter-sample [26, 44, 52], inter-class [26], or inter-channel [38, 62] relations via simple Gram matrices. To our best knowledge, no different forms of relations other than these have been proposed since 2022.

This paper fills this gap with a new kind of relations for KD – *inter-view* relations (Fig. 1c), which seamlessly and compactly integrate with previous inter-sample and inter-class relations. Our designs are motivated by two important observations made about RM methods in a set of pilot experiments: 1) RM methods are more susceptible to overfitting than IM methods; 2) RM methods are subject to an adverse gradient propagation effect. We empirically find that incorporating richer and more diverse relations into the matching objective helps mitigate both issues.

To this end, we generate *virtual views* of samples through simple transformations, followed by constructing *virtual affinity graphs* and transferring the *virtual relations* between real and virtual samples along the edges. In lieu of Gram matrices that suffer from significant knowledge loss [26, 44, 52], we preserve the raw relations along the secondary dimension as auxiliary knowledge which adds to the types and density of relational knowledge transferred. Moreover, we also prune our affinity graphs by striping away both redundant and unreliable edges to further alleviate the propagating gradients of spurious samples (Fig. 1d).

The above insights and remedies altogether lead to a novel *Virtual Relation Matching* (VRM) framework for KD. VRM is conceptually simple, easy to implement, and devoid of complicated training procedures. It is capable of transferring rich, sophisticated knowledge robust to overfitting and spurious signals. VRM sets new state-of-the-art performance on CIFAR-100 and ImageNet datasets for different ConvNet and Transformer architectures. Perhaps more significant is that VRM makes relation-based methods regain competitiveness and back in the lead over instance matching approaches across various tasks and settings. We will release the code and models to encourage further endeavours in relation-based KD.

To summarise, the contributions of this work include:

- We make an early effort to present comparative analyses of existing KD methods through the lens of training dynamics and sample-wise gradients, and identify overfitting and spurious gradient diffusion as two main cruxes in relational KD methods.
- We distill richer, more diverse relations by generating virtual views, constructing virtual affinity graphs, and matching virtual relations. We also for the first time

tackle relational KD with considerations of spurious samples and gradients by pruning redundant and unreliable edges, alongside designs to relax the matching criterion.

- We present the streamlined VRM framework for knowledge distillation, with extensive experimental results on a diversity of neural architectures and tasks to highlight its superior performance, alongside rigorous analyses on the soundness and efficiency of our designs.

2. Related Work

KD via instance-wise transfer. Knowledge distillation (KD) was first proposed in Hinton et al. [24], where the student is trained to match its predictions to those of the teacher for each sample. Follow-up works have mostly followed such *instance matching* (IM) paradigm, and can be categorised into logit (or prediction)-based and feature-based methods according to what representation is matched. Since Hinton et al. [24], logit-based KD has evolved from using adaptively-softened logits [35] or an ensemble of differently-softened [29] distributions to decoupling target- and non-target logits [61, 68] and applying logit transformation [49, 69] or consistency regularisation [66]. Methods such as TAKD [41] and DGKD [48] set up auxiliary ad-hoc networks between teacher and student to facilitate logit transfer. Early feature-based methods [1, 22, 46] directly minimise the distance between the feature maps at a specified layer in both teacher and student networks. AT [64] and CAT-KD [21] transfer the salient regions within features. Sophisticated distillation paths have been designed, such as “many-to-one” layer-wise matching [5] and “one-to-many” patch matching [36]. All these methods are based on instance-wise transfer of knowledge, either logits or features, and are herein referred to as the “IM” methods, as illustrated by Fig. 1a.

KD via relation transfer. Several works attempt to transfer instead mutual relations mined amongst the network outputs extracted from a batch of training instances. These *relation matching* (RM) methods usually involve constructing network outputs into compact relation representations that encodes rich higher-order information, as depicted in Fig. 1b. Different relation encoding functions may be used, including inter-sample [26, 40, 43–45, 52], inter-class [26], inter-channel [38], and inter-layer [40, 62], and contrastive [50] relations. To date, IM solutions have dominated KD with their superior performance, leading top-performing relation-based methods by considerable margins. While many new IM methods are found within the last two years, frustratingly few RM solutions are being proposed. In this work, we strive to close this gap with a new kind of relations for KD — inter-view virtual relations, and revive relation-based KD by making it overtake its IM counterparts.

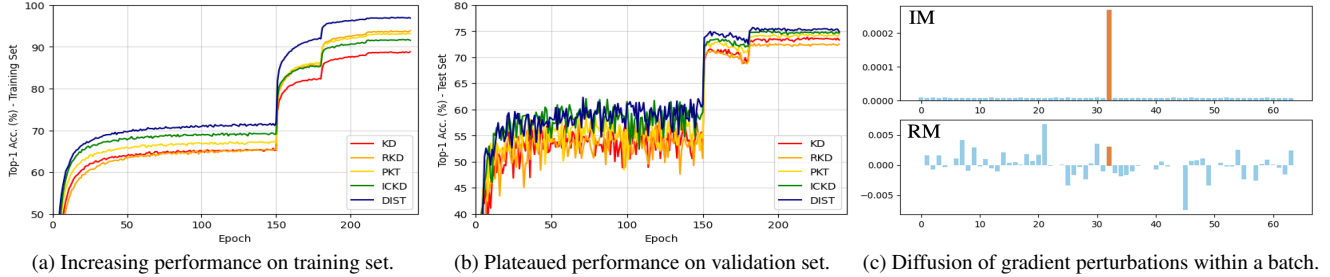


Figure 2. Pilot studies that reveal the overfitting and spurious gradient diffusion issues with RM-based KD.

Learning with virtual knowledge. While not a stand-alone research topic, learning with virtual knowledge finds relevance in a variety of learning-based problems. For instance, a commonly used paradigm in 3D vision tasks is to learn (or construct) from the raw data a virtual view or representation as auxiliary knowledge in solving the main task, which range from object reconstruction [3] and optical flow [2] to 3D semantic segmentation [32], monocular 3D object detection [11], and 3D GAN inversion [56]. More broadly, many data-efficient learning methods also share the spirit of utilising virtual knowledge. For instance, self-supervised learning methods generate virtual views of the unlabelled data to enable the learning of pretext tasks [9, 18]. Another popular paradigm is transformation-invariant representation learning [42, 47] in semi-supervised learning and domain adaptation. It enforces consistency between representations learnt for a raw sample and a virtual view of it. The virtual view is often obtained by applying semantic-preserving transformations to the raw sample [14, 15]. This work is more related to this later paradigm, but involves learning with virtual knowledge in a different context, via different approaches, and for a different problem.

3. Method

3.1. Preliminaries

KD methods generally employ a cross-entropy (CE) loss and a distillation loss to supervise the student learning. The CE loss is computed between the student logits \mathbf{z}_i^s for each sample and its ground-truth label \mathbf{y}_i . The distillation loss matches teacher and student outputs via a distance metric $\phi(\cdot)$. For instance, in vanilla KD [24] $\phi(\cdot)$ is the Kullback-Leibler divergence (KLD) between teacher logits \mathbf{z}^t and student logits \mathbf{z}^s :

$$\mathcal{L}_i^{\text{KD}} = \phi_{\text{KLD}}(\mathbf{z}_i^s, \mathbf{z}_i^t) = \tau^2 \sum_{j=1}^C \sigma_j(\mathbf{z}_i^t/\tau) \log \frac{\sigma_j(\mathbf{z}_i^t/\tau)}{\sigma_j(\mathbf{z}_i^s/\tau)},$$

where $\sigma(\cdot)$ is the Softmax operation with temperature parameter τ , and C is the number of classes. For feature-based methods, $\phi(\cdot)$ can be the mean squared error (MSE) between teacher and student feature maps for each instance [46], *i.e.*, $\mathcal{L}_i^{\text{KD}} = \phi_{\text{MSE}}(\mathbf{f}_i^s, \mathbf{f}_i^t)$.

For relation-based methods, a relation encoding function $\psi(\cdot)$ first abstracts teacher or student outputs of all instances within a training batch into a relational representation, before applying $\phi(\cdot)$ to match these relational representations between the teacher and the student. As an example, the KD objectives of DIST [26] take the general form of:

$$\mathcal{L}^{\text{KD}} = \phi(\psi(\mathbf{z}_1^s, \mathbf{z}_2^s, \dots, \mathbf{z}_B^s), \psi(\mathbf{z}_1^t, \mathbf{z}_2^t, \dots, \mathbf{z}_B^t)),$$

where B is the batch size, and subscript i of \mathcal{L}^{KD} is dropped as the loss is computed for a batch of instances. DIST uses both inter-class and inter-sample relation encoders as $\psi(\cdot)$.

3.2. Pilot Studies

Training dynamics of KD methods. We examine the training dynamics of different relation-based methods on CIFAR-100 with ResNet32×4→ResNet8×4 as the teacher-student pair. In Figs. 2a and 2b, we immediately notice that relational methods achieve significantly higher training accuracy, but they only marginally lead or even fall short in test accuracy compared to IM-based KD [24]. We hypothesise that relational methods are more prone to overfitting. This is expected given that the optimality of IM matching (cond. \mathcal{A}) implies the optimality of relation matching (cond. \mathcal{B}), while the converse does not hold. Concretely, $\mathcal{A} \Rightarrow \mathcal{B} \wedge \neg \mathcal{B} \Rightarrow \neg \mathcal{A}$. In other words, relation matching is a weaker and less constrained objective than IM, which makes the student more readily fit the teaching signals and not generalise well. Thus, we conclude that *C1: relation matching methods are more prone to overfitting*.

Gradient analysis of KD methods. We investigate the gradient patterns within a batch when a spurious sample produces a major misleading signal. To this end, we first generate two random vectors $\mathbf{x}, \mathbf{y} \sim \mathcal{N}(0, 1)$ for $\mathbf{x}, \mathbf{y} \in \mathbb{R}^{B \times D}$, where B is the batch size and D is the dimension of per-sample predictions, \mathbf{x} is taken as the sample-wise predictions, and \mathbf{y} the supervision signals. We then add a noise vector $\epsilon = c \cdot \mathbf{z}$ to \mathbf{x}_t , where $\mathbf{z} \sim \mathcal{N}(0, 1)$ and c is a scaling factor. In this case, $\mathbf{x}_t + \epsilon$ becomes a spurious prediction within our batch. We compute the loss from \mathbf{x} and \mathbf{y} using either IM or RM objectives, and consider the change in sample-wise gradients \mathbf{g} within the batch upon the injection of the spurious sample. Formally, we visualise

$$\Delta \mathbf{g} = \left[\left\| \frac{\partial \mathcal{L}}{\partial (\mathbf{x}'_i)} \right\|_2 - \left\| \frac{\partial \mathcal{L}}{\partial (\mathbf{x}_i)} \right\|_2 \right]_{i=1}^B,$$

s. t. $\mathbf{x}'_i = \mathbf{x}_i + \epsilon \cdot \mathbb{I}(i = t)$, $\mathcal{L} \in \{\mathcal{L}_{IM}, \mathcal{L}_{RM}\}$.

In Fig. 2c ($B = 64$ and $t = 32$), when the IM objective is used, only the spurious sample receives a prominent gradient. Whereas for an RM objective, many other samples receive significant gradients as they are directly connected to \mathbf{x}_t in the computational graph of the RM loss. In other words, the spurious signals produced by one malign prediction will propagate to and affect all samples within a batch (in fact, those closer to \mathbf{x}_t within the prediction manifold are more strongly affected). This means other sample-wise predictions will be significantly updated only to accommodate a malign prediction, even if they are already in relatively good shape. Through this investigation, we discover that *C2: relation matching methods are more prone to the adverse impact of spurious samples*.

For *C1*, common approaches to combat overfitting include the incorporation of richer learning signals and regularisation, which for RM-based KD methods means richer relations constructed and transferred. For *C2*, an intuitive solution is to identify and suppress the effect of spurious predictions or relations or to slacken the matching criterion. Guided by these principles, let us move on to formally build up our method. The remaining parts of this section present step-by-step descriptions of individual design choices that in tandem constitute our method.

3.3. Constructing Inter-Sample Relations

We first construct relation graph \mathcal{G}^{IS} that encodes inter-sample affinity within a batch of sample predictions $\{\mathbf{z}_i\}_{i=1}^B$. Different from [43, 52], our relations are constructed from predicted logits which embed more compact categorical knowledge. We use the pairwise distance between instance-wise predictions within a batch as our measure of affinity. Existing methods leverage the Gram matrices [26, 44, 45, 52] to encode inter-sample relations, but we find that this leads to collapsed inter-class knowledge via the inner product operation. Instead, our pairwise distance preserves the inter-class knowledge along the secondary dimension (*i.e.*, the class dimension), which enables such information to be explicitly transferred as auxiliary knowledge alongside the matching of inter-sample relations.

Thus, we have constructed a dense relation graph \mathcal{G}^{IS} , which comprises B vertices and $B \times B$ edges: $\mathcal{G}^{IS} = (\mathcal{V}^{IS}, \mathcal{E}^{IS})$. Each vertex in \mathcal{G}^{IS} represents the prediction vector $\mathbf{z} \in \mathbb{R}^C$ for one instance within a batch, and is connected to all instances within the batch including itself. The attribute of edge $\mathcal{E}_{i,j}^{IS}$ connecting vertices i and j describes the class-wise relations between the predictions of instances i and j . In practice, we can organise all edges into matrix $\mathcal{E}^{IS} \in \mathbb{R}^{B \times B \times C}$, in which:

$$\mathcal{E}_{i,j}^{IS} = \frac{\mathbf{z}_i - \mathbf{z}_j}{\|\mathbf{z}_i - \mathbf{z}_j\|_2} \in \mathbb{R}^C \quad \text{for } i, j \in [1, B], \quad (1)$$

where we empirically find that normalisation along the secondary dimension helps regularise relations and improves performance (see Sec. 4.3). Concretely, \mathcal{E} encodes inter-sample class-wise relations within a batch of B training samples. Our method of encoding inter-sample affinity is different from and more effective than previous methods that leverage Gram matrices [26, 43, 44, 52] or third-order angular distances [43].

3.4. Constructing Inter-Class Relations

Although \mathcal{G}^{IS} densely encodes rich inter-sample relations within a batch, it fails to explicitly model inter-class patterns that are also beneficial structured knowledge [26]. We propose to build and transfer a novel inter-class batch-wise relation graph $\mathcal{G}^{IC} = (\mathcal{V}^{IC}, \mathcal{E}^{IC})$, instead of Gram matrices in the inner product space in [26]. The construction of \mathcal{G}^{IC} mirrors that of \mathcal{G}^{IS} . Vertices in \mathcal{G}^{IC} are the class-wise logit vectors $\mathbf{w} \in \mathbb{R}^B$. Each edge in $\mathcal{E}^{IC} \in \mathbb{R}^{C \times C \times B}$ embeds the pairwise difference between the i -th and j -th per-class vectors.

$$\mathcal{E}_{i,j}^{IC} = \frac{\mathbf{w}_i - \mathbf{w}_j}{\|\mathbf{w}_i - \mathbf{w}_j\|_2} \in \mathbb{R}^B \quad \text{for } i, j \in [1, C].$$

Our inter-class relations preserve the batch-wise discrepancies by treating them as a dimension of additional knowledge (reciprocal to the case of inter-sample relations), which is unlike any other previous methods [26]. We demonstrate in Tab. 7 that our formulation of inter-sample and inter-class relations by preserving the raw affinity knowledge along the secondary dimension performs significantly better than previous relation encoders $\psi(\cdot)$ via Gram matrices or third-order angular distances. Furthermore, We will show in Sec. 4.3 that knowledge transfer with our formulation works reasonably well with various distance metrics $\phi(\cdot)$.

3.5. Constructing Virtual Relations

For each prediction \mathbf{z}_i within a batch $\{\mathbf{z}_i\}_{i=1}^B$, we create a virtual view of it, denoted as “ $\tilde{\mathbf{z}}_i$ ”, by applying semantic-preserving transformations to original image \mathbf{x}_i . While other common image transformation operations are applicable, we choose RandAugment [15] that applies stochastic image transformations. With our batch of predictions augmented into $\{\mathbf{z}_i, \tilde{\mathbf{z}}_i\}_{i=1}^B$, we can construct a larger inter-sample edge matrix $\mathcal{E}^{IS} \in \mathbb{R}^{2B \times 2B \times C}$ and a larger inter-class edge matrix $\mathcal{E}^{IC} \in \mathbb{R}^{C \times C \times 2B}$. From the perspective of sample views, our new \mathcal{E}^{IS} encompasses inter-class batch-wise prediction affinity between within-view instance predictions. Our new \mathcal{E}^{IS} essentially encode three types of knowledge, namely relations amongst real views (denoted

Teacher Student	Venue	ResNet56	ResNet32×4	WRN-40-2	WRN-40-2	VGG13	ResNet32×4	VGG13	ResNet50	WRN-40-2
		ResNet20	ResNet8×4	WRN-16-2	WRN-40-1	VGG8	ShuffleNetV2	MobileNetV2	MobileNetV2	ShuffleNetV1
Teacher		72.34	79.42	75.61	75.61	74.64	79.42	74.64	79.34	75.61
Student		69.06	72.50	73.26	71.98	70.36	71.82	64.60	64.60	70.50
<i>Feature-based</i>										
FitNets [46]	ICLR'15	69.21	73.50	73.58	72.24	71.02	73.54	64.16	63.16	73.73
AT [64]	ICLR'17	70.55	73.44	74.08	72.77	71.43	72.73	59.40	58.58	73.32
VID [1]	CVPR'19	70.38	73.09	74.11	73.30	71.23	73.40	65.56	67.57	73.61
CRD [50]	ICLR'20	71.16	75.51	75.48	74.14	73.94	75.65	69.63	69.11	76.05
SRRL [58]	ICLR'21	71.13	75.33	75.59	74.18	73.44	-	-	-	-
PEFD [10]	NeurIPS'22	70.07	76.08	76.02	74.92	74.35	-	-	-	-
CAT-KD [21]	CVPR'23	71.05	76.91	75.60	74.82	74.65	78.41	69.13	71.36	77.35
TaT [36]	CVPR'22	71.59	75.89	76.06	74.97	74.39	-	-	-	-
ReviewKD [8]	CVPR'21	71.89	75.63	76.12	75.09	74.84	77.78	70.37	69.89	77.14
NORM [39]	ICLR'23	71.35	76.49	75.65	74.82	73.95	78.32	69.38	71.17	77.63
FCFD [37]	ICLR'23	71.96	76.62	76.43	75.46	75.22	78.18	70.65	71.00	77.99
<i>Logit-based</i>										
KD [24]	arXiv'15	70.66	73.33	74.92	73.54	72.98	74.45	67.37	67.35	74.83
TAKD [41]	AAAI'20	70.83	73.81	75.12	73.78	73.23	74.82	67.91	68.02	75.34
CTKD [35]	AAAI'23	71.19	73.79	75.45	73.93	73.52	75.31	68.46	68.47	75.78
NKD [61]	ICCV'23	70.40	76.35	75.24	74.07	74.86	76.26	70.22	70.76	75.96
DKD [68]	CVPR'22	71.97	76.32	76.24	74.81	74.68	77.07	69.71	70.35	76.70
LSKD [49]	CVPR'24	71.43	76.62	76.11	74.37	74.36	75.56	68.61	69.02	-
TTM [69]	ICLR'24	71.83	76.17	76.23	74.32	74.33	76.55	69.16	69.59	75.42
MLLD [29]	CVPR'23	72.19	77.08	76.63	75.35	75.18	78.44	70.57	71.04	77.44
TGeoKD [25]	ICLR'24	72.98	77.27	-	75.43	-	76.89	-	-	77.05
CRLD [66]	MM'24	72.10	77.60	76.45	75.58	75.27	78.27	70.39	71.36	-
<i>Relation-based</i>										
RKD [43]	CVPR'19	69.61	71.90	73.35	72.22	71.48	73.21	64.52	64.43	72.21
PKT [44]	ECCV'18	70.34	73.64	74.54	73.45	72.88	74.69	67.13	66.52	73.89
CCKD [45]	CVPR'19	69.63	72.97	73.56	72.21	70.71	71.29	64.86	65.43	71.38
SP [52]	ICCV'19	69.67	72.94	73.83	72.43	72.68	74.56	66.30	68.08	74.52
ICKD [38]	ICCV'21	71.76	75.25	75.64	74.33	73.42	-	-	-	-
DIST [26]†	NeurIPS'22	71.75	76.31	-	74.73	-	77.35	68.50	68.66	76.40
VRM	-	72.09	78.76	77.47	76.46	76.19	79.34	71.66	72.30	78.62
<i>Abs. Improvements</i>		<i>+3.03</i>	<i>+6.26</i>	<i>+4.21</i>	<i>+4.48</i>	<i>+5.83</i>	<i>+7.52</i>	<i>+7.06</i>	<i>+7.70</i>	<i>+8.12</i>

Table 1. Results for same- and different-architecture teacher-student pairs on CIFAR-100. †: using re-trained, stronger teachers.

as “real-real”), relations amongst virtual views (“virtual-virtual”), and relations between pairs of real and virtual views (“real-virtual”). For instance, a real-virtual edge that connects real vertex m and virtual vertex n in \mathcal{E}^{IS} is computed as $\mathcal{E}_{m,n}^{IS} = \frac{\mathbf{z}_m - \tilde{\mathbf{z}}_n}{\|\mathbf{z}_m - \tilde{\mathbf{z}}_n\|_2} \in \mathbb{R}^C$.

3.6. Pruning into Sparse Graphs

Pruning redundant edges. The augmented \mathcal{E}^{IS} in Sec. 3.5 contains $2B \times 2B$ edges in dense connections, leading to quadrupled memory and computational overheads. For better efficiency, we prune \mathcal{G}^{IS} into sparse graphs. Noticing that \mathcal{E}^{IS} is symmetric along its diagonals, we first prune its redundant half, which leads to up to 50% reduction in the number of edges. We also remove intra-view edges as we empirically find them redundant and harm knowledge transfer. We postulate this is because virtual views are laden with most of the essential knowledge of the real views they are generated from, which makes the former also redundant. This step leads to a further $2\times$ edge reduction. For \mathcal{G}^{IC} , we decompose the augmented batch of predictions of size $2B$ into a real-view batch and a virtual-view batch, each of size B , and in lieu use the inter-sample batch-wise affinity vectors between them as its vertices. Compared to their

original intra-view formulation of size $2B$ in Sec. 3.5, this design encodes purely cross-view affinity knowledge with halved parameters. Our graphs now become sparse and the remaining edges can again be rearranged into compact matrices: $\mathcal{E}^{ISV} \in \mathbb{R}^{B \times B \times C}$ and $\mathcal{E}^{ICV} \in \mathbb{R}^{C \times C \times B}$, both encoding purely cross-view virtual relational knowledge.

Pruning unreliable edges. To mitigate the diffusive effect of spurious predictions discovered earlier, we further identify and prune the unreliable edges. In previous graph learning works, the absolute certainty of two vertices are often used to determine the reliability of an edge. For instance, REM [7] computes the reliability of an edge as the mean of the maximum predicted probabilities of two samples (*i.e.*, two vertices). However, we argue this could bias the learning towards easy samples. Instead, we measure the discrepancy between two predictions. The larger this discrepancy, the more unreliable the relation constructed from them. Mathematically, the unreliable edge pruning criterion is given by:

$$\mathcal{E}_{i,j}^{ISV} = \emptyset \quad \text{if} \quad H(\mathbf{z}_i^s, \tilde{\mathbf{z}}_j^s) > P_m \quad (2)$$

where $H(\cdot)$ computes the joint entropy (JE) between two predictions and P_m is the m -th percentile within the batch. Note that the criterion is enforced on student predictions, which results in adaptive and dynamic pruning as different edges get pruned in each iteration, which improves learning.

3.7. Further Designs for Relaxed Matching

We implement further designs to mitigate the issues pinpointed in Sec. 3.2, namely logit adaptors and logit normalisation. Note that we do not claim these designs as our main contribution. Instead, we show they indeed work well with our proposed method, but the most significant performance gains are still from our main designs in previous sections. These findings are nonetheless non-trivial, given that this is the *first time MLP adaptors and ZSNorm are reported to bring performance gains when applied to RM*. More discussions are found in Supplementary Material.

3.8. Full Objective

With \mathcal{G}^{IS} and \mathcal{G}^{IC} constructed for both teacher and student predictions, our VRM objective matches \mathcal{E}^{ISV} and \mathcal{E}^{ICV} between teacher and student via distance metric $\phi(\cdot)$. Formally, $L_{vrm}^{ISV} = \phi(\mathcal{E}_S^{ISV}, \mathcal{E}_T^{ISV})$ and $L_{vrm}^{ICV} = \phi(\mathcal{E}_S^{ICV}, \mathcal{E}_T^{ICV})$. The full objective is a weighted combination of the CE loss and the proposed VRM losses:

$$L_{total} = L_{ce} + \alpha L_{vrm}^{ISV} + \beta L_{vrm}^{ICV} \quad (3)$$

where L_{ce} is the CE loss applied to student’s predictions of both real and virtual views and supervised by GT labels; α and β are scalars to balance different loss terms.

4. Experiments

4.1. Experimental Settings

Our method is evaluated on the CIFAR-100 [31] and ImageNet [17] datasets for image recognition. All experimental configurations strictly follow the standard practice in prior works. More details are provided in Supplementary Material.

4.2. Main Results

Results on CIFAR-100. For *same-architecture KD*, (left of Tab. 1), VRM surpasses all previous relation-based methods across all teacher-student pairs by large margins. Noticeably, VRM significantly outperforms even the strongest feature-based method, FCFD. On average, it also performs much better than top logit-based methods such as TGeoKD and MLLD. These results are significant, given that IM methods are known to be naturally more adapt at homogeneous pairs. For *different-architecture KD*, which RM methods are supposed to be more competent with, VRM readily surpasses *all* RM and IM methods with notable margins. These results highlight VRM’s versatility on both homogeneous and heterogeneous KD pairs.

Teacher Student	Venue	ResNet34 ResNet18	ResNet50 MobileNetV1
Teacher Student		73.31/91.42 69.75/89.07	76.16/92.86 68.87/88.76
<i>Feature-based</i>			
AT [64]	ICLR’17	70.69/90.01	69.56/89.33
OFD [22]	ICCV’19	70.81/89.98	71.25/90.34
CRD [50]	ICLR’20	71.17/90.13	71.37/90.41
CAT-KD [21]	CVPR’23	71.26/90.45	72.24/91.13
SimKD [6]	CVPR’22	71.59/90.48	72.25/90.86
ReviewKD [8]	CVPR’21	71.61/90.51	72.56/91.00
SRRL [58]	ICLR’21	71.73/90.60	72.49/90.92
PEFD [10]	NeurIPS’22	71.94/90.68	73.16/91.24
FCFD [37]	ICLR’23	72.24/90.74	73.37/91.35
<i>Logit-based</i>			
KD [24]	arXiv’15	70.66/89.88	68.58/88.98
TAKD [41]	AAAI’20	70.78/90.16	70.82/90.01
CTKD [35]	AAAI’23	71.51/-	90.47/-
DKD [68]	CVPR’22	71.70/90.41	72.05/91.05
NKD [61]	ICCV’23	71.96/-	72.58/-
SDD [55]	CVPR’24	71.14/90.05	72.24/90.71
MLLD [29]	CVPR’23	71.90/90.55	73.01/91.42
TTM [69]	ICLR’24	72.19/-	73.09/-
LSKD [49]	CVPR’24	72.08/90.74	73.22/91.59
TGeoKD [25]	ICLR’24	72.89/91.80	72.46/90.95
CRLD [66]	MM’24	72.37/90.76	73.53/91.43
<i>Relation-based</i>			
FSP [62]	CVPR’17	70.58/89.61	-
RKD [43]	CVPR’19	71.34/90.37	71.32/90.62
CCKD [45]	CVPR’19	70.74/-	-
ICKD [38]	ICCV’21	72.19/90.72	-
DIST [26]†	NeurIPS’22	72.07/90.42	73.24/91.12
VRM	-	72.93/91.03	74.16/91.78
<i>Abs. Improvements</i>		<i>+3.18/1.96</i>	<i>+5.29/3.02</i>

Table 2. Results on ImageNet. †: with retrained, stronger teachers.

Student	BL	KD	AT	SP	LG	AutoKD	LSKD	VRM
DeiT-Ti	65.08	73.25	73.51	67.36	78.15	78.58	78.55	79.52 ^{+14.4}
T2T-ViT-7	69.37	74.15	74.01	72.26	78.35	78.62	78.43	78.88 ^{+9.51}
PiT-Ti	73.58	75.47	76.03	74.97	78.48	78.51	78.76	79.25 ^{+5.67}
PVT-Ti	69.22	74.66	77.07	70.48	77.48	73.60	78.43	79.42 ^{+10.2}

Table 3. Results for ConvNet-to-ViT distillation on CIFAR-100. BL: baseline.

Results on ImageNet. VRM surpasses all feature- and relation-based methods on this large-scale dataset, shown in Tab. 2. The advantage of VRM is again more apparent over the heterogeneous pair (*i.e.*, ResNet50→MobileNetV2), whereby it produces the highest performance and *for the first time hits 74.0% Top-1 accuracy*. Notably, VRM outperforms strong competitors such as FCFD, PEFD, and NORM with comparable or even less computational overheads as compared in Tab. 7.

Results for ConvNet-to-ViT Distillation We train a ResNet56 teacher on CIFAR-100 and distill its knowledge into various ViT students (*i.e.*, DeiT [51], T2T-ViT [63], PiT [23], and PVT [54]). Tab. 3 suggests VRM sets new record under this set-up for different ViT architectures. By simply replacing the vanilla KD objective with our VRM

Component	ResNet32×4 VGG13	
	ResNet8×4 VGG8	
Baseline	72.50	70.36
+ Match $\{\mathcal{E}^{IS}\}$	75.64	74.08
+ Match $\{\mathcal{E}^{IS}, \mathcal{E}^{IC}\}$	75.94	74.47
+ Match $\{\mathcal{E}^{ISV}\}$	77.63	75.30
+ Match $\{\mathcal{E}^{ISV}, \mathcal{E}^{ICV}\}$	78.38	75.56
+ Pruning	78.76	76.19

Table 4. Ablation of major designs in VRM.

α	32	64	128	256	512	
Acc. (%)	78.03	78.13	78.76	78.32	77.84	
β	8	16	32	64	128	
Acc. (%)	78.40	78.51	78.76	78.86	78.60	
n	0	1	2	3	4	5
Acc. (%)	77.92	78.38	78.76	78.55	78.43	78.50

Table 5. Effect of different α , β , and n .

Matching Choice	ResNet32 ×4 VGG13		ResNet50
	ResNet8×4	VGG8	MobileNetV2
Match \emptyset	72.50	70.36	68.33
Match $\{\mathcal{E}\}$	78.76	76.19	72.30
Match $\{\mathcal{E}, \mathcal{V}\}$	78.63	75.60	70.97
Match $\{\mathcal{V}\}$	78.46	75.77	68.33

Table 6. Effect of matching graph vertices.

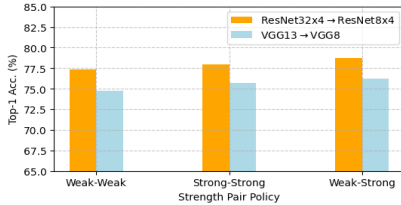


Figure 3. Effect of different difficulty pairs.

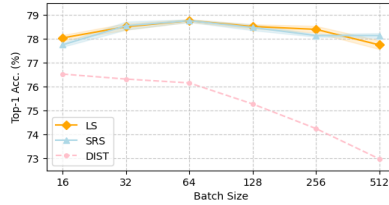


Figure 4. Robustness to varying B .

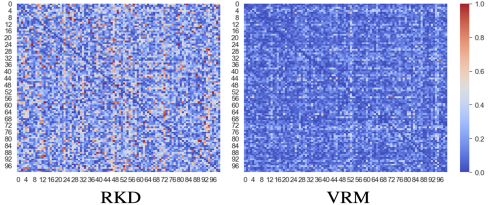


Figure 5. Teacher-student prediction discrepancies.

and making no other modifications, VRM improves DeiT-Ti by 14.44%, leading RM-based SP by 12.16% and even surpassing AutoKD [34] with AutoML search.

4.3. Ablation Studies

Ablations of main design choices. In Tab. 4, starting from the baseline where only the CE loss is applied, we gradually incorporate each of our designs. As shown, each extra design consistently brings performance gains, which corroborate the validity of individual design choices.

Effect of varying hyperparameters. According to Tab. 5, VRM works generally well with α and β in a reasonable range. Larger α and β may produce better results for certain KD pairs but worse results for others. Hence, we default α to 128 and β to 32 in favour of generalisation.

Effect of different real-virtual difficulty gaps. We probe into the effect of different difficulty gaps in our real-virtual relation matching formulation. We first tune RandAugment’s parameter n , which controls the number of transformations sampled to create the virtual view. The larger n , the more difficult the image becomes and the larger discrepancy between the logits of both views. From Tab. 5, $n = 2$ works best, whereas other values also report competitive results compared to state-of-the-arts. We also experiment with different strength pairs in Fig. 3 and find that cross-strength matching performs best. Overall, we conclude that 1) a moderate difficulty gap leads to optimal performance, and 2) difficulty gaps are significant to the success of VRM.

Robustness to varying batch sizes. Inter-sample relational methods are known to be sensitive to B , the number of samples within a training batch. We examine how robust VRM is against varying B . To adjust the learning rate accord-

ingly, we consider two LR scaling rules: linear LR scaling [19] and square root LR scaling [9]. From Fig. 4, VRM yields competitive results across a wide range of B values. In contrast, the performance of DIST [26] deteriorates significantly as B varies.

4.4. Further Analysis

Teacher-student prediction discrepancy. We compute the mean discrepancy (Manhattan used) between teacher’s averaged prediction distribution for each class and that of student on the CIFAR-100 validation set. From Fig. 5, VRM pulls student’s predictions significantly closer to teacher’s compared to RKD, while both methods do not involve direct IM matching objectives. This can be attributed to our designs such as cross-view regularisation and graph pruning that substantially improve generalisation.

Visualisation of embedding space. We conduct t-SNE analysis on student penultimate layer embeddings learnt via different methods. As presented in Fig. 8, VRM leads to more compact per-class clusters with clearer inter-class separation and less stray points. These imply our method induces better features in student for the downstream task.

Analysis of training dynamics. Figs. 6a and 6b plot the per-epoch training and validation set accuracies throughout training. VRM maintains a all-time lead in both training and validation performance, with faster convergence. Besides, while VRM’s lead in training performance tapers off towards the end of training, it remains more substantial, if not further enlarging, in validation performance, which highlights its superior generalisation properties. This analysis also shows our designs are effective in mitigating the issues with existing RM methods identified in the pilot studies.

Analysis of loss landscape. We further analyse the gener-

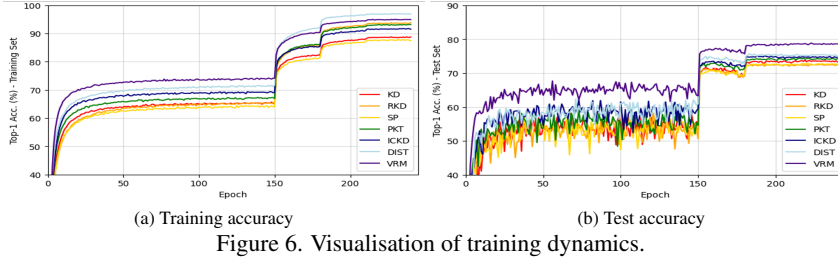


Figure 6. Visualisation of training dynamics.

$\psi(\cdot)$	Shape of Rel. Matrix	Method	ResNet32×4VGG13 ResNet8×4	ResNet50 VGG8	MobileNetV2
Gram matrices	$[B, B]$ & $[C, C]$	CC, SP, PKT, DIST	77.31	75.12	70.28
Angle-wise relations	$[B, B, B]$	RKD	77.14	75.09	69.65
ISV & ICV	$[B, B, C]$ & $[C, C, B]$	VRM	78.76	76.19	72.30

Figure 7. Comparison of different $\psi(\cdot)$.

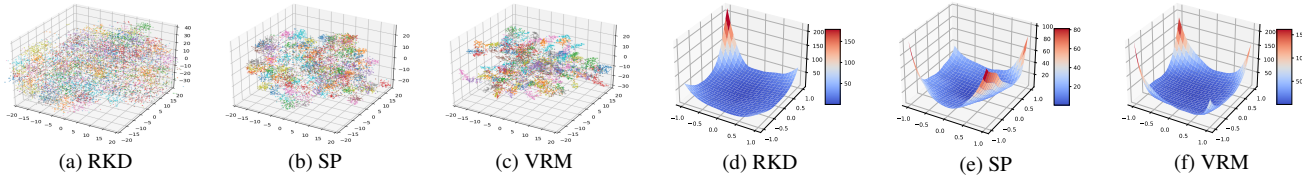


Figure 8. t-SNE (a-c) and loss landscape (d-f) visualisations for ResNet8×4 students distilled with a ResNet32×4 teacher on CIFAR-100 via different methods.

Method	KD	RKD	ICKD	DIST	CRD	ReviewKD	SDD	LSKD	MLLD	NORM	PEFD	FCFD	VRM
Train. Time (ms)	24.9	31.0	28.0	27.2	41.2	39.9	34.2	27.1	57.2	35.1	36.2	56.4	47.2
Peak GPU Mem. Usage (MB)	323	330	381	330	1418	1042	690	330	576	1806	701	953	579

Table 7. Training efficiency of different distillation methods.

alisation and convergence properties of our method through the lens of visualised loss landscape [33]. From Fig. 8, VRM has the widest and flattest region of minima – typical hint of better model generalisation and robustness; this wide convexity basin surrounded by salient pikes in various directions indicates excellent convergence properties.

Training efficiency. From Tab. 7, VRM’s training speed and GPU memory usage are both within a reasonable range compared with existing algorithms. Notably, VRM is more efficient than top-performing feature-based [10, 37, 39] and logit-based [29, 55] methods. Our method does not introduce any additional overheads at inference.

Vertex matching. VRM matches edges \mathcal{E}^{ISV} and \mathcal{E}^{ICV} which carry relational knowledge. By extension, we can naturally expect vertices \mathcal{V} to be also transferred. From Tab. 6, matching vertices is not as effective. The advantage of matching relations (*i.e.*, edges) is more pronounced for heterogeneous KD pairs such as ResNet50→MobileNetV2. Adding vertex matching to the proposed edge matching does not improve but instead degrades performance. We argue this is because introducing vertex matching objectives make the matching criterion more stringent which is against our motivation of using more slackened matching.

Effect of different relation encoding functions. Tab. 7 compares our proposed relation encoding scheme with existing ones. To demonstrate the superiority of our formulation, we substitute it with existing Gram matrices [26, 44, 45, 52] or angle-wise relations [43]. Results show that our method yields significantly better performance, validating

the superiority of VRM’s formulation of relations.

Role of transformation operations. We emphasise the *strong performance of VRM is not a simple outcome of the transformations* involved. This can be verified by the results in Fig. 3 where using only the default weak transformations in existing methods (*i.e.*, random crop and horizontal flip) for both views achieves 77.38% accuracy (denoted as “Weak-Weak”), compared to the baseline of 75.64% (Tab. 4) and 71.90% of RKD with exactly the same transformations. In fact, in the case of “Weak-Weak”, both views still differ because of the stochastic operations used. *The success of VRM lies exactly in this discrepancy*, where cross-view regularisation comes into crucial play.

5. Conclusion

This paper presents VRM, a novel knowledge distillation framework that constructs and transfers virtual relations. Our designs are motivated by a set of pilot experiments, from which we identified two main cruxes with existing relation-based KD methods: their tendency to overfit and susceptibility to adverse gradient propagation. A series of tailored designs are developed and are shown to successfully mitigate these issues. We have conducted extensive experiments on different tasks and multiple datasets and verified VRM’s validity and superiority in diverse settings, whereby VRM consistently demonstrates state-of-the-art performance. We hope that this work could renew the community’s interest in relation-based knowledge distillation, and encourage more systematic reassessment of the design principles of such solutions.

References

- [1] Sungsoo Ahn, Shell Xu Hu, Andreas Damianou, Neil D. Lawrence, and Zhenwen Dai. Variational information distillation for knowledge transfer. In *CVPR*, 2019. 2, 5
- [2] Filippo Aleotti, Matteo Poggi, and Stefano Mattoccia. Learning optical flow from still images. In *CVPR*, 2021. 3
- [3] Joao Carreira, Abhishek Kar, Shubham Tulsiani, and Jitendra Malik. Virtual view networks for object reconstruction. In *CVPR*, 2015. 3
- [4] Jiahao Chang, Shuo Wang, Hai-Ming Xu, Zehui Chen, Chenhongyi Yang, and Feng Zhao. Detrdistill: A universal knowledge distillation framework for detr-families. In *ICCV*, 2023. 1
- [5] Defang Chen, Jian-Ping Mei, Yuan Zhang, Can Wang, Zhe Wang, Yan Feng, and Chun Chen. Cross-layer distillation with semantic calibration. In *AAAI*, 2021. 2
- [6] Defang Chen, Jian-Ping Mei, Hailin Zhang, Can Wang, Yan Feng, and Chun Chen. Knowledge distillation with the reused teacher classifier. In *CVPR*, 2022. 6
- [7] Peibin Chen, Tao Ma, Xu Qin, Weidi Xu, and Shuchang Zhou. Data-efficient semi-supervised learning by reliable edge mining. In *CVPR*, 2020. 5
- [8] Pengguang Chen, Shu Liu, Hengshuang Zhao, and Jiaya Jia. Distilling knowledge via knowledge review. In *CVPR*, 2021. 5, 6
- [9] Ting Chen, Simon Kornblith, Mohammad Norouzi, and Geoffrey Hinton. A simple framework for contrastive learning of visual representations. In *ICML*, 2020. 3, 7
- [10] Yudong Chen, Sen Wang, Jiajun Liu, Xuwei Xu, Frank de Hoog, and Zi Huang. Improved feature distillation via projector ensemble. In *NeurIPS*, 2022. 5, 6, 8
- [11] Yi-Nan Chen, Hang Dai, and Yong Ding. Pseudo-stereo for monocular 3d object detection in autonomous driving. In *CVPR*, 2022. 3
- [12] Zehui Chen, Zhenyu Li, Shiquan Zhang, Liangji Fang, Qin-hong Jiang, and Feng Zhao. Bevdistill: Cross-modal bev distillation for multi-view 3d object detection. In *ICLR*, 2023. 1
- [13] Zhiyu Chong, Xinzhu Ma, Hong Zhang, Yuxin Yue, Haojie Li, Zhihui Wang, and Wanli Ouyang. Monodistill: Learning spatial features for monocular 3d object detection. *ICLR*, 2022. 1
- [14] Ekin D. Cubuk, Barret Zoph, Dandelion Mane, Vijay Vasudevan, and Quoc V. Le. Autoaugment: Learning augmentation strategies from data. In *CVPR*, 2019. 3
- [15] Ekin Dogus Cubuk, Barret Zoph, Jon Shlens, and Quoc Le. Randaugment: Practical automated data augmentation with a reduced search space. In *NeurIPS*, 2020. 3, 4
- [16] Kaiwen Cui, Yingchen Yu, Fangneng Zhan, Shengcai Liao, Shijian Lu, and Eric P Xing. Kd-dlgan: Data limited image generation via knowledge distillation. In *CVPR*, 2023. 1
- [17] Jia Deng, Wei Dong, Richard Socher, Li-Jia Li, Kai Li, and Li Fei-Fei. Imagenet: A large-scale hierarchical image database. In *CVPR*, 2009. 6
- [18] Spyros Gidaris, Praveer Singh, and Nikos Komodakis. Un-supervised representation learning by predicting image rotations. In *ICLR*, 2018. 3
- [19] P Goyal. Accurate, large minibatch sgd: training imagenet in 1 hour. *arXiv preprint arXiv:1706.02677*, 2017. 7
- [20] Yuxian Gu, Li Dong, Furu Wei, and Minlie Huang. Minillm: Knowledge distillation of large language models. In *ICLR*, 2024. 1
- [21] Ziyao Guo, Haonan Yan, Hui Li, and Xiaodong Lin. Class attention transfer based knowledge distillation. In *CVPR*, 2023. 2, 5, 6
- [22] Byeongho Heo, Jeessoo Kim, Sangdoon Yun, Hyojin Park, Nojun Kwak, and Jin Young Choi. A comprehensive overhaul of feature distillation. In *ICCV*, 2019. 2, 6
- [23] Byeongho Heo, Sangdoon Yun, Dongyoon Han, Sanghyuk Chun, Junsuk Choe, and Seong Joon Oh. Rethinking spatial dimensions of vision transformers. In *ICCV*, 2021. 6
- [24] Geoffrey Hinton, Oriol Vinyals, and Jeff Dean. Distilling the knowlegde in a neural network. In *arXiv:1503.02531*, 2015. 1, 2, 3, 5, 6
- [25] Chengming Hu, Haolun Wu, Xuan Li, Chen Ma, Jun Yan, Boyu Wang, and Xue Liu. Exploiting trilateral geometry for knowledge distillation. In *ICLR*, 2024. 1, 5, 6
- [26] Tao Huang, Shan You, Fei Wang, Chen Qian, and Chang Xu. Knowledge distillation from a stronger teacher. In *NeurIPS*, 2022. 2, 3, 4, 5, 6, 7, 8
- [27] Yuge Huang, Jiayang Wu, Xingkun Xu, and Shouhong Ding. Evaluation-oriented knowledge distillation for deep face recognition. In *CVPR*, 2022. 1
- [28] Sujin Jang, Dae Ung Jo, Sung Ju Hwang, Dongwook Lee, and Daehyun Ji. Stxd: structural and temporal cross-modal distillation for multi-view 3d object detection. *NeurIPS*, 2024. 1
- [29] Ying Jin, Jiaqi Wang, and Dahua Lin. Multi-level logit distillation. In *CVPR*, 2023. 2, 5, 6, 8
- [30] Minha Kim, Shahroz Tariq, and Simon S Woo. Fretal: Generalizing deepfake detection using knowledge distillation and representation learning. In *CVPR*, 2021. 1
- [31] Alex Krizhevsky. Learning multiple layers of features from tiny images. 2009. 6
- [32] Abhijit Kundu, Xiaoqi Yin, Alireza Fathi, David Ross, Brian Brewington, Thomas Funkhouser, and Caroline Pantofaru. Virtual multi-view fusion for 3d semantic segmentation. In *ECCV*, 2020. 3
- [33] Hao Li, Zheng Xu, Gavin Taylor, Christoph Studer, and Tom Goldstein. Visualizing the loss landscape of neural nets. *NeurIPS*, 2018. 8
- [34] Lujun Li, Peijie Dong, Zimian Wei, and Ya Yang. Automated knowledge distillation via monte carlo tree search. In *ICCV*, 2023. 7
- [35] Zheng Li, Xiang Li, Lingfeng Yang, Borui Zhao, Renjie Song, Lei Luo, Jun Li, and Jian Yang. Curriculum temperature for knowledge distillation. In *AAAI*, 2023. 2, 5, 6
- [36] Sihao Lin, Hongwei Xie, Bing Wang, Kaicheng Yu, Xiaojun Chang, Xiaodan Liang, and Gang Wang. Knowledge distillation via the target-aware transformer. In *CVPR*, 2022. 2, 5
- [37] Dongyang Liu, Meina Kan, Shiguang Shan, and Xilin Chen. Function-consistent feature distillation. In *ICLR*, 2023. 1, 5, 6, 8

- [38] Li Liu, Qingle Huang, Sihao Lin, Hongwei Xie, Bing Wang, Xiaojun Chang, and Xiaodan Liang. Exploring inter-channel correlation for diversity-preserved knowledge distillation. In *ICCV*, 2021. 2, 5, 6
- [39] Xiaolong Liu, Lujun Li, Chao Li, and Anbang Yao. Norm: Knowledge distillation via n-to-one representation matching. In *ICLR*, 2023. 1, 5, 8
- [40] Yufan Liu, Jiajiong Cao, Bing Li, Chunfeng Yuan, Weiming Hu, Yangxi Li, and Yunqiang Duan. Knowledge distillation via instance relationship graph. In *CVPR*, 2019. 2
- [41] Seyed-Iman Mirzadeh, Mehrdad Farajtabar, Ang Li, Nir Levine, Akihiro Matsukawa, and Hassan Ghasemzadeh. Improved knowledge distillation via teacher assistant. In *AAAI*, 2020. 2, 5, 6
- [42] Ishan Misra and Laurens van der Maaten. Self-supervised learning of pretext-invariant representations. In *CVPR*, 2020. 3
- [43] Wonpyo Park, Dongju Kim, Yan Lu, and Minsu Cho. Relational knowledge distillation. In *IEEE TMM*, 2019. 1, 2, 4, 5, 6, 8
- [44] Nikolaos Passalis and Anastasios Tefas. Learning deep representations with probabilistic knowledge transfer. In *ECCV*, 2018. 2, 4, 5, 8
- [45] Baoyun Peng, Xiao Jin, Jiaheng Liu, Shunfeng Zhou, Yichao Wu, Yu Liu, Dongsheng Li, and Zhaoning Zhang. Correlation congruence for knowledge distillation. In *CVPR*, 2019. 2, 4, 5, 6, 8
- [46] Adriana Romero, Nicolas Ballas, Samira Ebrahimi Kahou, Antoine Chassang, Carlo Gatta, and Yoshua Bengio. Fitnets: Hints for thin deep nets. In *ICLR*, 2015. 1, 2, 3, 5
- [47] Kihyuk Sohn, David Berthelot, Chun-Liang Li, Zizhao Zhang, Nicholas Carlini, Ekin D. Cubuk, Alex Kurakin, Han Zhang, and Colin Raffel. Fixmatch: Simplifying semi-supervised learning with consistency and confidence. In *NeurIPS*, 2020. 3
- [48] Wonchul Son, Jaemin Na, Junyong Choi, and Wonjun Hwang. Densely guided knowledge distillation using multiple teacher assistants. In *ICCV*, 2021. 2
- [49] Shangquan Sun, Wenqi Ren, Jingzhi Li, Rui Wang, Rui Wang, and Xiaochun Cao. Logit standardization in knowledge distillation. In *CVPR*, 2024. 2, 5, 6
- [50] Yonglong Tian, Dilip Krishnan, and Phillip Isola. Contrastive representation distillation. In *ICLR*, 2020. 2, 5, 6
- [51] Hugo Touvron, Matthieu Cord, Matthijs Douze, Francisco Massa, Alexandre Sablayrolles, and Herve Jegou. Training data-efficient image transformers & distillation through attention. In *ICML*, 2021. 6
- [52] Frederick Tung and Greg Mori. Similarity-preserving knowledge distillation. In *ICCV*, 2019. 1, 2, 4, 5, 8
- [53] Tao Wang, Li Yuan, Xiaopeng Zhang, and Jiashi Feng. Distilling object detectors with fine-grained feature imitation. In *CVPR*, 2019. 1
- [54] Wenhai Wang, Enze Xie, Xiang Li, Deng-Ping Fan, Kaitao Song, Ding Liang, Tong Lu, Ping Luo, and Ling Shao. Pyramid vision transformer: A versatile backbone for dense prediction without convolutions. In *ICCV*, 2021. 6
- [55] Shicai Wei, Chunbo Luo, and Yang Luo. Scale decoupled distillation. In *CVPR*, 2024. 6, 8
- [56] Jiaxin Xie, Hao Ouyang, Jintan Piao, Chenyang Lei, and Qifeng Chen. High-fidelity 3d gan inversion by pseudo-multi-view optimization. In *CVPR*, 2023. 1, 3
- [57] Chuanguang Yang, Helong Zhou, Zhulin An, Xue Jiang, Yongjun Xu, and Qian Zhang. Cross-image relational knowledge distillation for semantic segmentation. In *CVPR*, 2022. 1
- [58] Jing Yang, Brais Martinez, Adrian Bulat, and Georgios Tzimiropoulos. Knowledge distillation via softmax regression representation learning. In *ICLR*, 2021. 5, 6
- [59] Longrong Yang, Xianpan Zhou, Xuewei Li, Liang Qiao, Zheyang Li, Ziwei Yang, Gaoang Wang, and Xi Li. Bridging cross-task protocol inconsistency for distillation in dense object detection. In *ICCV*, 2023. 1
- [60] Zhendong Yang, Zhe Li, Xiaohu Jiang, Yuan Gong, Zehuan Yuan, Danpei Zhao, and Chun Yuan. Focal and global knowledge distillation for detectors. In *CVPR*, 2022. 1
- [61] Zhendong Yang, Ailing Zeng, Zhe Li, Tianke Zhang, Chun Yuan, and Yu Li. From knowledge distillation to self-knowledge distillation: A unified approach with normalized loss and customized soft labels. In *ICCV*, 2023. 2, 5, 6
- [62] Junho Yim, Donggyu Joo, Jihoon Bae, and Junmo Kim. A gift from knowledge distillation: Fast optimization, network minimization and transfer learning. In *CVPR*, 2017. 2, 6
- [63] Li Yuan, Yunpeng Chen, Tao Wang, Weihao Yu, Yujun Shi, Zi-Hang Jiang, Francis EH Tay, Jiashi Feng, and Shuicheng Yan. Tokens-to-token vit: Training vision transformers from scratch on imagenet. In *ICCV*, 2021. 6
- [64] Sergey Zagoruyko and Nikos Komodakis. Paying more attention to attention: Improving the performance of convolutional neural networks via attention transfer. In *ICLR*, 2017. 2, 5, 6
- [65] Bo Zhang, Jiacheng Sui, and Li Niu. Foreground object search by distilling composite image feature. In *ICCV*, 2023. 1
- [66] Weijia Zhang, Dongnan Liu, Weidong Cai, and Chao Ma. Cross-view consistency regularisation for knowledge distillation. In *ACM MM*, 2024. 2, 5, 6
- [67] Weijia Zhang, Dongnan Liu, Chao Ma, and Weidong Cai. Alleviating foreground sparsity for semi-supervised monocular 3d object detection. In *WACV*, 2024. 1
- [68] Borui Zhao, Quan Cui, Renjie Song, Yiyu Qiu, and Jiajun Liang. Decoupled knowledge distillation. In *CVPR*, 2022. 2, 5, 6
- [69] Kaixiang Zheng and En-Hui Yang. Knowledge distillation based on transformed teaching matching. In *ICLR*, 2024. 2, 5, 6
- [70] Shengchao Zhou, Weizhou Liu, Chen Hu, Shuchang Zhou, and Chao Ma. Unidistill: A universal cross-modality knowledge distillation framework for 3d object detection in bird's-eye view. In *CVPR*, 2023. 1

We express our sincere gratitude to all reviewers (R1:gFtf, R2:32xp, R3:uUpu) for their valuable feedback. We appreciate their recognition of our novelty (R2, R3), motivating studies (R2, R3), strong performance (R1, R2, R3), and comprehensive analysis (R1, R2, R3). We address reviewers’ comments in detail as follows:

R1(Q1): VRM further clarified. We highlight that VRM encompasses at least two distinct innovations. 1) Put aside virtual relations, **our affinity graph itself represents a contribution**, distinct from all existing relation formulations (see shape & type comparisons in Tab. 8). Concretely, our \mathcal{E} encodes inter-sample class-wise (hence [B,B,C]) and inter-class sample-wise ([C,C,B]) affinities, substantially different from CC, SP, PKT, and DIST ([B,B] and [C,C]) and RKD ([B,B,B]). Our designed affinity alone ($\{\mathcal{E}^{IS}, \mathcal{E}^{IC}\}$ in Tab. 5) already surpasses prior RM methods. 2) **Virtual affinity transfer.** Unlike any prior RM methods constrained by a limited set of correlations, VRM benefits from a potentially unbounded amount of *diverse* virtual relations, with *controllable* regularisation strength, which directly addresses overfitting in current RM methods.

In short, compared to prior RM methods, VRM 1) constructs affinity graphs in **different formulation** (inter-sample class-wise & inter-class sample-wise), 2) encodes knowledge in **different intensity** (several times higher), and 3) transfers knowledge of **different nature** (virtual). Due to these vast distinctions, VRM offers much higher performance and extra desirable properties, (e.g., robustness to B , whereas DIST collapses; see Fig.4). Also see R2(Q2).

It’s noteworthy that pruning in VRM is **different from the common “pruning” concept in model compression**. Our redundancy pruning is handily implemented as a real-virtual broadcast subtraction without explicit trimming steps. Our uncertainty pruning adaptively drops unreliable edges, which is *first of its kind* in the larger KD literature.

R1(Q2): Latest IM methods. We compared latest IM methods in 2024 (LSKD, TTM, TGeoKD, SDD). We **couldn’t find other IM/feature-based methods in top venues in 2024** by the time of submission. The best IM methods so far are FCFD (feature) and TGeoKD (logit). Tabs. 1-2, 10-11 show VRM greatly surpasses them. We’ll stay tuned and update any new IM methods when possible.

R1(Q3): Efficiency. Thanks for this point! We analyse it in Tab. A. Results confirm our motivation that redund. edge pruning (REP) boosts efficiency at minimal performance cost, whereas uncert. pruning (UEP) trades minimal efficiency cost for performance. We’ll revise our manuscript.

R2(Q1): Relations to existing RM methods. Please kindly see R1(Q1) for clarifications on VRM’s differences from prior RM methods and potential confusion.

R2(Q2): Justification of effectiveness. *Empirically*, we can justify VRM alleviates the issues of overfitting (Fig. 6) and spurious gradients (Fig. A) (improved training and con-

Policy	R32x4-R8x4			V13-V8 W40-2-SNv2	
	Acc. (%)	Batch Time (s)	Peak Mem. (MB)	Acc. (%)	Acc. (%)
w/o pruning	78.38	61.4	34.3	75.56	78.45
+ REP	78.46	46.3	13.6	75.30	78.41
+ UEP	78.76	47.2	13.1	76.19	78.62

Table A. Effect of prunings and their efficiency.

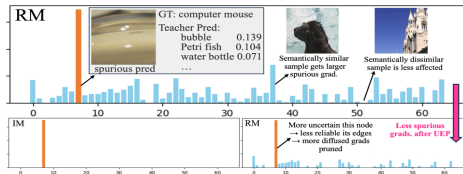


Figure A. Pilot studies for real KD training on ImageNet.

vergence also evident from loss landscapes). *Theoretically*, VRM’s alleviation of overfitting finds theoretical ground in Information Bottleneck Theory (IBT) [?]. By matching the real-virtual relations, student is enforced to grasp compact shared knowledge (e.g., virtual edges) while robust to volatile distracting information (e.g., variances in virtual nodes). An orthogonal perspective is the transfer of diverse relations, where extensive theories on how data augmentation regularises training come in handy (we may view VRM as a sort of “relation augmentation”). We’ll expand empirical/theoretical interpretations in our final manuscript.

R2(Q3): Further details. Virtual relations are built and matched as follows. We’ll add full pseudocode for clarity.

```
G_tea = tea_r.unsqueeze(0) - tea_v.unsqueeze(1) # [B,B,C] (similarly for G_stu)
loss_isv = loss(G_tea, G_stu, reduce='none') # [B,B,C] (similarly for loss_icv)
```

R3(Q1): Extra pilot studies. As suggested, in Fig. A we present pilot studies in more practical set-ups by using: 1) real spurious signals in real KD learning, instead of manual noise, and 2) ImageNet instead of CIFAR-100.

R3(Q2): More on pruning. Unreliable edge mask \mathcal{M}_{uep} is computed from \mathcal{E}_S . An edge-wise loss is computed between \mathcal{E}_S and \mathcal{E}_T , and is multiplied with \mathcal{M}_{uep} edge-wise. So yes, \mathcal{M}_{uep} prunes same parts of \mathcal{E}_S and \mathcal{E}_T . We’ll add pseudocode to make all operations crystal-clear. For their effect, see Tab. A and Fig. A. We’ll also add visuals and discuss 1) correlations between removed edges and the confidence/correctness of their nodes; 2) how the number of removed edges and their confidence evolve during training.

R3(Q3): Impact of data augmentation. In [?], “increased number of samples” is essentially due to their use of data augmentation to match more IM pairs. Hence, VRM also increased the number of samples like [?] *per se*. Yet, VRM uses these “extra” virtual nodes to transfer an “increased diversity of relations”. Tab. 7 shows VRM’s performance increases and then saturates with larger n (i.e., effectively “more samples”), which aligns with results in [?]. Fig. 3 also studies various strength pairs of data augmentation.

R3(Q4): Further details. [25] uses a GT (cross-entropy) loss and a KD (KLD) loss. Graphs for detection are built similarly, except that per-sample relation becomes per-proposal, i.e., \mathcal{E}^{ISV} ’s shape changes from $[B, B, C]$ to $[N, N, C]$, where N is the number of proposals in a batch. We’ll include further details in our revised manuscript.